

PAPER • OPEN ACCESS

Magnetic field design for miniature pulse Penning ion source

To cite this article: N V Mamedov *et al* 2020 *Plasma Sources Sci. Technol.* **29** 025001

View the [article online](#) for updates and enhancements.



IOP | ebooks™

Bringing you innovative digital publishing with leading voices to create your essential collection of books in STEM research.

Start exploring the collection - download the first chapter of every title for free.

Magnetic field design for miniature pulse Penning ion source

N V Mamedov^{1,2,4} , A V Gubarev¹, V I Zverev^{1,2,3} , S P Maslennikov^{1,2} ,
A A Solodovnikov¹, A A Uzzvolok¹ and D I Yurkov^{1,2}

¹ Dukhov Automatics Research Institute (VNIIA), Federal State Unitary Enterprise, 22, Sushevskaya Ul., Moscow 127055, Russia

² National Research Nuclear University MEPhI, 31, Kashirskoye Sh., Moscow 115409, Russia

³ Physics department, M.V. Lomonosov Moscow State University, GSP-1, Leninskie Gory, Moscow, 119991, Russia

E-mail: m_nikitos@mail.ru

Received 23 September 2019, revised 17 December 2019

Accepted for publication 3 January 2020

Published 4 February 2020



CrossMark

Abstract

Magnetic field configuration for a miniature pulse Penning ion source was designed in this work. The amplitude-time characteristics of discharge and extracted currents were investigated as a function of gas pressure for various magnetic field magnitude and configuration. An effect of magnetic field configuration on the Penning's discharge modes and characteristics of the extraction current impulse were experimentally shown. Stable operation modes of the ion source were found in this work. Also the appropriate ranges of working gas pressure and magnetic field configuration were demonstrated, at which the current pulse of the extracted ions had a quasi-rectangular form. For better understanding real magnetic fields distributions of within the discharge cell magnetic field have been calculated in COMSOL software.

Keywords: Penning ion source, Penning discharge modes, amplitude-time characteristics, gas sealed neutron tube

1. Introduction

The Penning ion source (PIS) in the miniature linear accelerator was first used in 1937 by Penning and Moubis to obtain the D–D nuclear reaction and generate neutrons [1]. Due to simple design and power supply system, as well as reliable operation at low working-gas pressures, the PIS are widely used in the neutron generation systems [2].

Schematic diagram of this ion source type is the following: two cathodes (cathode and anticathode with the extracting aperture) and ring (or cylinder) anode are placed in the longitudinal (parallel to the system axis) magnetic field (see figure 1). Cathodes are negative potential to the anode. The pile-up of magnetic field parallel to the system axis

results in curvature of the electron paths. Thus, the electron path in the discharge chamber is extended increasing efficiency of working gas ionization within the discharge cell.

There are several discharge modes depending on pressure (p), magnetic field (B) and anode voltage (U_a): Townsend mode (or ignition region)—T, low magnetic field—LMF, high magnetic field—HMF, transition mode—TM, high pressure—HP and glow discharge region—GD [3, 4]. The modes foremost affect the real potential distribution (in radial and axial directions) within the discharge cell and determine the ion and electron component values of the discharge current, and, hence, affect the extracted current.

The experiments described in most recent [5–10] use the permanent cylindrical magnets around the anode and assume that magnetic field is homogeneous within the discharge cell and directed strictly along the axis. At the same time, the references devoted to PIS development for miniature linear accelerators [11–17] demonstrate a trend to use the end magnets. The end magnet generates a mildly divergent magnetic field in the discharge cell. A use of inhomogeneous field enables to reduce the overall source dimensions and

⁴ Author to whom any correspondence should be addressed.



Original content from this work may be used under the terms of the [Creative Commons Attribution 4.0 licence](https://creativecommons.org/licenses/by/4.0/). Any further distribution of this work must maintain attribution to the author(s) and the title of the work, journal citation and DOI.

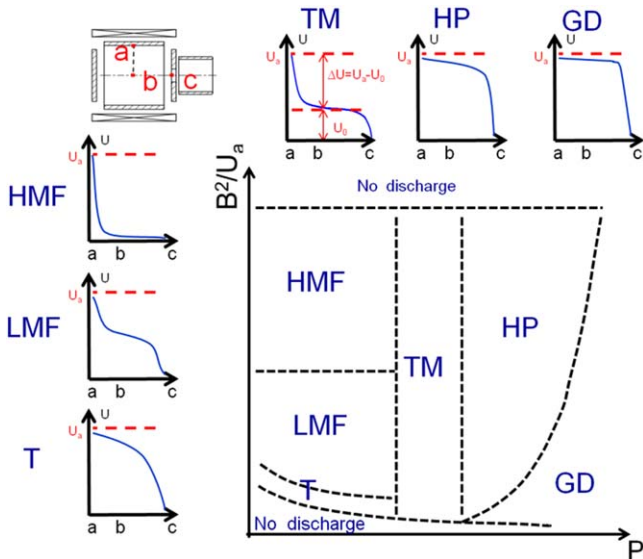


Figure 1. Penning discharge modes and their potential profiles [3, 4].

decrease the operating gas pressure (up to $\sim 10^{-4}$ Torr). And there are both different combinations of the magnetic system and the magnetic inserts applied to the source construction.

Unfortunately, there are nearly no explanations for choosing of magnetic field induction in these papers. It widely varies from 0.03 to 0.35 T. Often there is no data on the absolute values and distribution of the magnetic field within the discharge cell in these papers (sometimes the magnetic field characteristics are shown for cathode region only). Ion sources of different dimensions with different magnetic field configurations were described in these papers. Also the parameters of specific experiments differ from each other. Under these circumstances, it is extremely difficult to compare the experimental data obtained from different articles and use the acquired in it results and conclusions derived in practice.

In this paper the optimal magnetic field configuration for the miniature pulse PIS (previously described in [18–22]) is selected using physical experiment. For this purpose, the amplitude-time characteristics of the discharge and extracted currents are investigated as a function of magnetic field magnitude and distribution generated by a solenoid. For development PIS for miniature linear accelerator (for gas sealed neutron tube) the following quantitative optimization criteria are chosen: (1) the maximum of extracted ion current I_{ex} at a constant extracted potential U_{ex} , (2) the minimum of discharge current I_d at a constant anode potential U_a , (3) the minimum of current delay time t_{delay} and rise of the current pulse t_{front} , (4) the minimum of work pressure p . Another words goal aims were maximum ion-extraction coefficient (the ratio of the extracted current to the discharge current I_{ex}/I_d) at the lowest pressure and rectangular form of extracted ion current. These parameters are most important, when PIS applied in high-yield neutron generator, which can be used in neutron radiography, oil well logging and neutron activation analysis [23, 24].

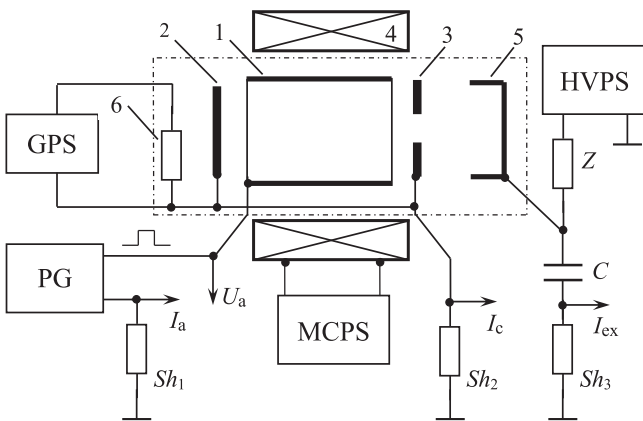


Figure 2. Power supply for the system used to investigate discharge modes in PIS: (1)-anode, (2)-cathode, (3)-anticathode with extracting aperture, (4)-solenoid, (5)-accelerating electrode and target, (6)-getter (gas storage).

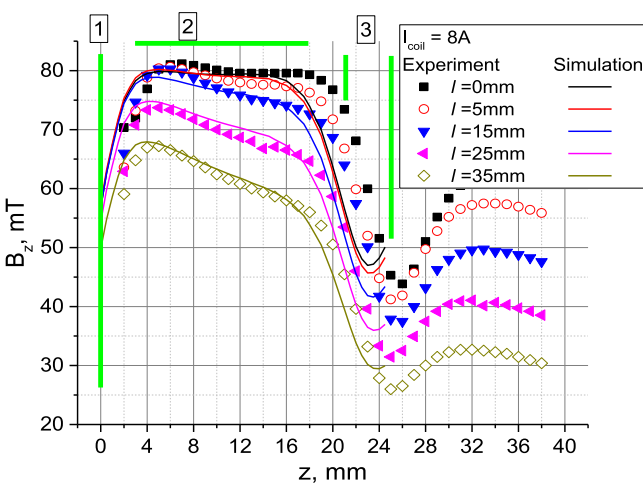


Figure 3. Distribution of magnetic field $B_z(z)$ along the PIS axis within the discharge region for different solenoid positions and different coil current values. Electrode positions: (1)-cathode, (2)-anode, (3)-anticathode.

2. Review of Penning discharge modes

Penning discharge modes diagram and their potential profiles (in radial and axial directions) within the discharge cell are shown at figure 1. The mode boundaries are schematic. The modes of Penning discharge with cylindrical anode and constant anode voltage have been described in [3, 4].

There is Townsend discharge at low B and p . The space-charge is still small and the center potential U_o is close to U_a . As the magnetic field is increased (LMF mode), the electron density increases in comparison with ions concentration. This is because the average time for ion to reach a cathode is much less than the electron confinement time. The potential profile is deformed by a cloud of electron, spread out over the whole discharge cell. In HMF mode (at high B) the electron density is sufficiently large. The potential drop ($\Delta U = U_a - U_o$) occurs in an anode sheath and the center potential is cathode potential. In [3] is shown that discharge current (I_d) is proportional to pressure and radial potential drop. So I_d is

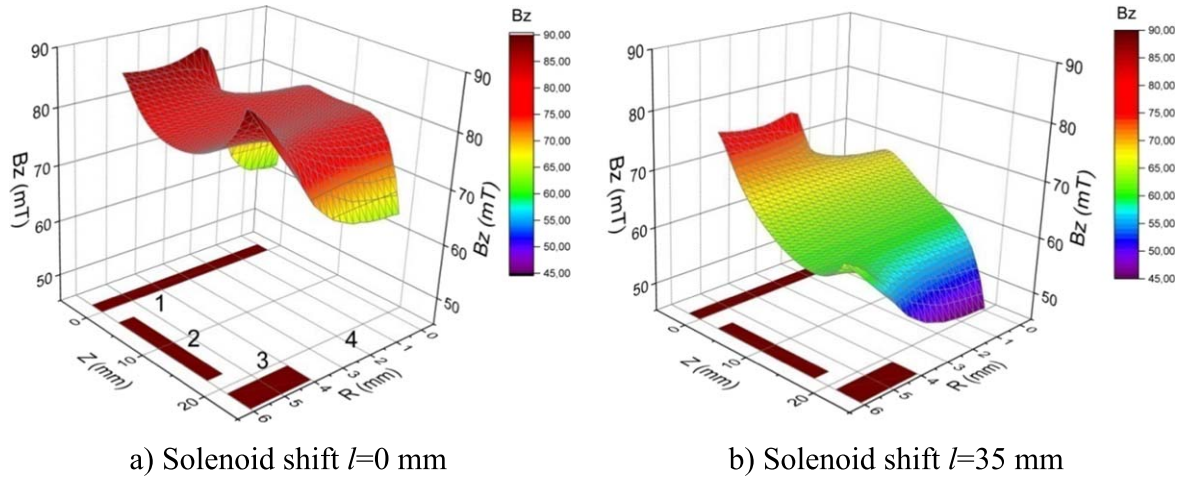


Figure 4. $B_z(r, z)$ magnetic field distribution in the discharge gap simulated in the COMSOL for different solenoid positions and coil current, $I_{\text{coil}} = 8$ A. Electrode positions: (1)-cathode, (2)-anode, (3)-anticathode, (4)-extracting aperture.

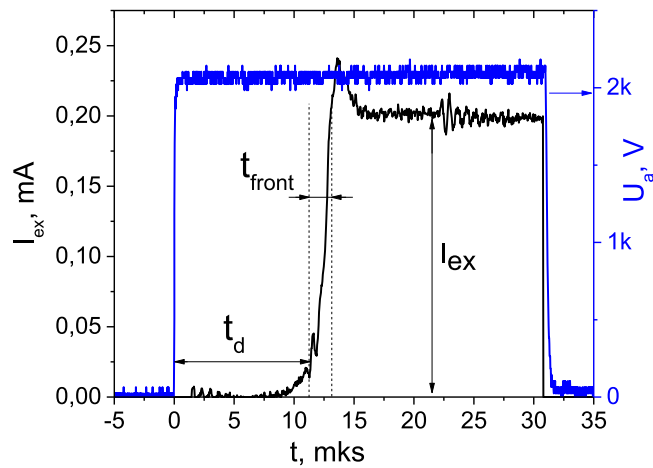


Figure 5. A typical extraction current and anode voltage pulse shape. $U_a = 2.0$ kV, $f = 10$ kHz, $t_{\text{vp}} = 30$ μs , $P = 4$ mTorr, $I_{\text{coil}} = 10$ A, $l = 35$ mm.

maximum during transition from LMF mode to the HMF mode.

As p is raised, the electron loss rate and ionization process increase consequently the electron and ion densities tended to be approximately equal. The potential drop decreases, the plasma switches to a quasineutral regime (TM-mode). This mode is observed to be unstable and the instability has not been good investigated yet [4]. Assuming that electron density remains limited a further pressure increase (HP-mode) above to disappearance of the anode sheath. The discharge current rises rapidly. The discharge switches to HP-mode in which the voltage drop occurs in cathode sheaths. Potential profile becomes similar to that of a glow discharge. When p continues rise and magnetic field is no longer essential, the discharge switches to glow discharge with unusual electrode geometry.

In this paper dynamics of discharge ignition and discharge operation mode at a pulsed anode voltage supply are investigated.

3. Experimental setup description

3.1. Experimental setup and measurement methods

The high vacuum setup for the PIS main parameters measurements is described [22]. The maximum residual pressure is 10^{-6} Torr. For develop PIS for gas-sealed neutron tube, only deuterium gas was used in these experiments. The operating pressure varied from 0.1 to 10 mTorr. The relative error of the pressure measurements is no more than 45% [22]. The PIS operates both in pulse and stationary modes of anode power supply [22]. Pulse power supply of the experiment setup, used to investigate discharge modes in PIS, are shown in figure 2. The solid-state pulse generator generates up to 4 kV pulses on the PIS anode with repetition rate of 20 kHz. Extracting voltage is set by a high-voltage power supply unit. The winding of magnetic coil generating the magnetic field in the Penning cell is energized from the DC power supply (MCPS). A regulated power supply is applied for heating the getter (gas storage in the PIS).

3.2. Magnetic system variants or magnetic field simulation

A current solenoid was used to generate an axially symmetric magnetic field (of various induction and configuration) in the PIS. The solenoid was chosen for convenience to adjust induction of the magnetic field with uniform radial and azimuthal component. The anode size of the investigated PIS is about $15 \times \text{Ø}12$ mm (distance between cathodes is about 20 mm, see figures 3 and 4), which has been described in previous papers [19, 21]. Anode and body of PIS were made of stainless steel, cathode and anticathode were made of magnetically conductive material—Kovar (Cobalt-nickel alloy). These electrodes significantly affect on the magnetic field distribution inside the discharge cell. The magnetic field distribution was measured for different values of current flowing through the solenoid coil and for different position of the discharge cell center towards the solenoid center (l). Figure 3 demonstrates the results of numerical simulation in

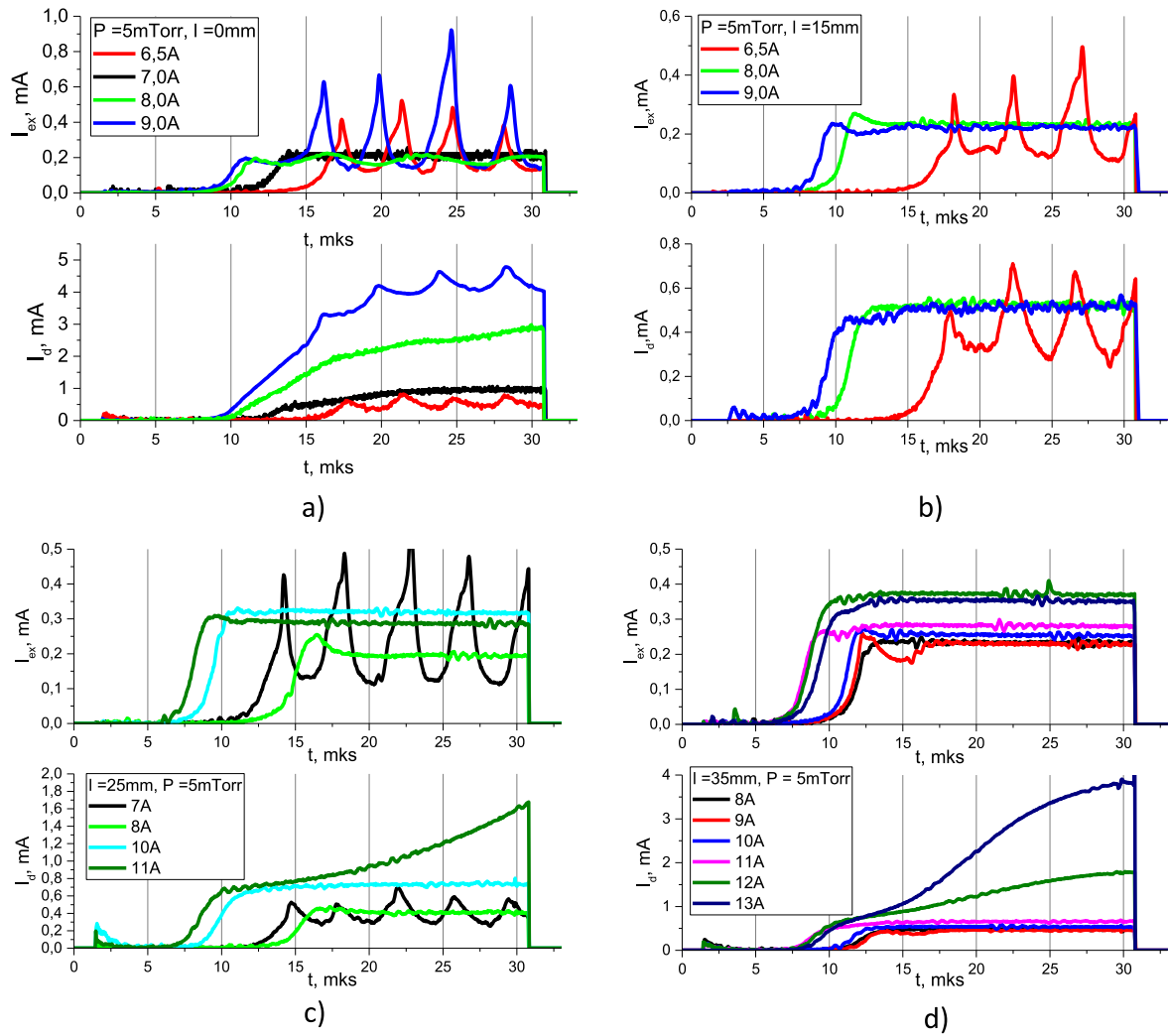
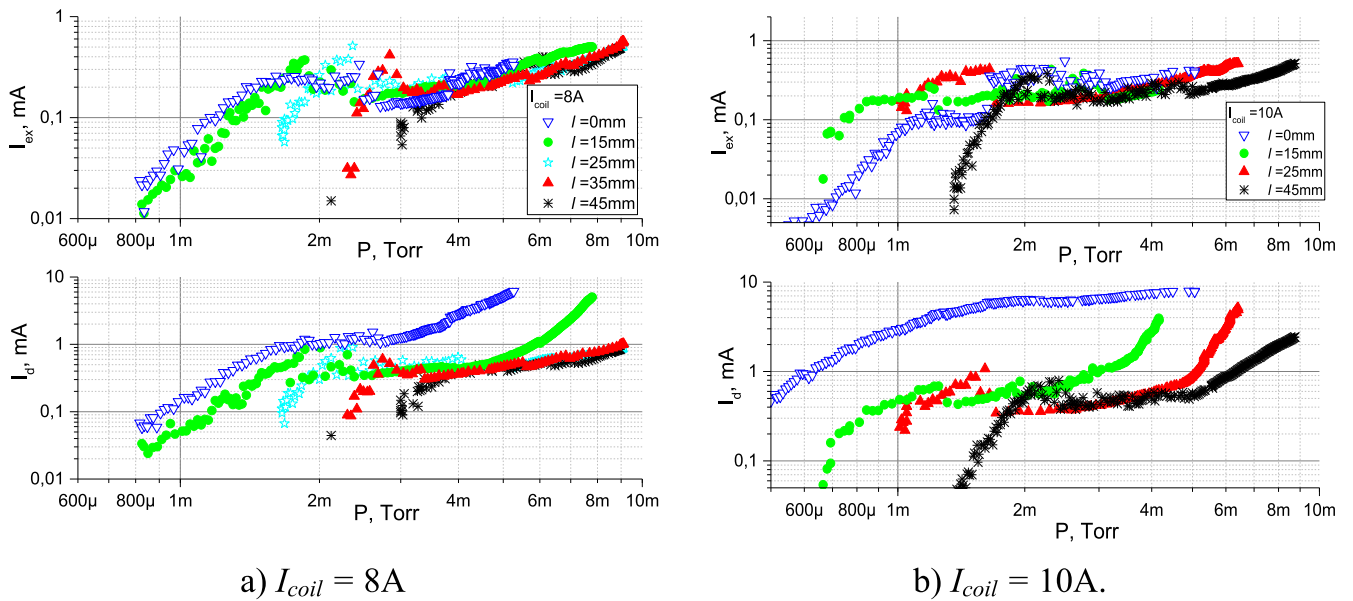


Figure 6. Typical examples of current pulse waveforms: I_d —discharge current and I_{ex} —ion current extracted from the PIS. $U_a = 2.0$ kV, $U_{ex} = -20$ kV.



a) $I_{coil} = 8A$

b) $I_{coil} = 10A.$

Figure 7. Discharge current I_d and extracted current I_{ex} , as a function of pressure for different solenoid positions and coil currents: (a) $I_{coil} = 8$ A and (b) $I_{coil} = 10$ A.

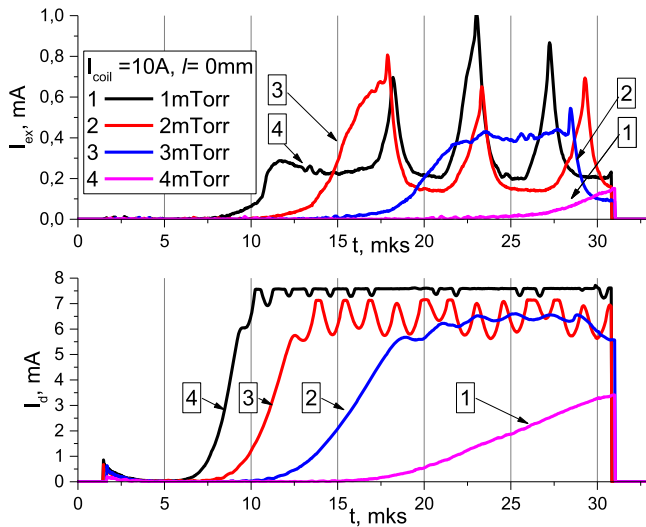


Figure 8. Typical examples of current pulse waveforms: I_d —discharge current and I_{ex} —ion current extracted from the PIS for homogenous and high magnetic field.

the COMSOL and magnetic field measurements on the axis of PIS discharge gap for several solenoid locations.

As it can be seen, at $l = 0$ mm there is a relatively homogenous distribution of magnetic field along the cell axis. If the solenoid is shifted along the axis towards the cathode for $l = 15$ mm, the ‘weakly’ inhomogeneous field distribution is formed with drop of magnetic induction towards the anticathode by about 10%. For example, if coil current is $I_{coil} = 8$ A, the magnetic field induction (for shift $l = 15$ mm) near ‘cathode’ edge of the anode is $B_z \sim 80$ mT ($z = 3$ mm) and near ‘anticathode’ edge— $B_z \sim 72$ mT ($z = 18$ mm). If the solenoid shifts for $l = 35$ mm relative to the PIS center, the magnetic field inhomogeneity is more obvious and magnetic induction in the cell drops by about 20%. For example, if the coil current is $I_{coil} = 10$ A, the magnetic field induction (for shift $l = 35$ mm) near ‘cathode’ edge of the anode is $B_z \sim 85$ mT ($z = 3$ mm) and near ‘anticathode’ edge— $B_z \sim 70$ mT ($z = 18$ mm). The figures shows the electrode coordinates in a green form of segments.

Figure 4 presents the 3D distributions of $B_z(z, r)$ magnetic field component within the discharge cell obtained by simulation in the COMSOL Multiphysics. The solenoid coil current is $I_{coil} = 8$ A. When the solenoid shift is 0 cm (figure 3(a)), the field in the discharge gap is homogenous, $B_z = 78$ mT, and its relative change along radius (r) does not exceed 5%. The B_z induction rise at $r > 4$ mm is caused by magnetic cathode and anticathode materials and, hence, by field closure. At the same time, when the solenoid is shifted for 35 mm (figure 3(b)), the field in the discharge gap goes extremely down towards anticathode. The $B_z(r \neq 0)$ changes by about 30% from 67 to 46 mT.

There are two reasons for investigating such extreme cases of magnetic field distribution. On the one hand, the uniform magnetic field parallel to the anode ensures free migration of the electrons along the magnetic field lines, making the ionization more probable and thus increasing the current. On the other hand, the research results presented in

[25] show that, the inhomogeneous magnetic field generated, which goes down towards the extracting aperture, forms a region with high emission ability.

4. Experimental results

In our previous works [18, 19], the energy distribution and mass-charge composition of ions emitted from the discharge under different discharge modes were investigated. The correspondence with discharge current bursts and potential drop (up to 50% of anode voltage) is established. It is shown that the content of atomic hydrogen ions does not exceed 10% with an increase in the anode voltage from 1 to 3.5 kV and the power invested in the discharge (from 0.2 to 3 W). It can be seen from [18, 19] that at the anode voltage of 2 kV the atom-molecule ratio varies within 6%–8%. We suppose that the variation in the distribution of the magnetic field within our working range (50–200 mT) should not have significant effect on the atom-molecule ratio and the latter one should not exceed 10%. It should be noted, that more significant influence on the atom-molecule ratio is exerted by the substitution of the cathode materials but maximum of atom-molecule ratio is 16% [5].

In this paper experimental studies of the PIS operation modes were carried out in the pulse-periodic power supply mode with pulse repetition rate $f = 10$ kHz and width $t_{vp} = 30$ μ s typical for this device type [2]. The voltage applied to the PIS anode is $U_a = 2.0$ kV, the voltage applied to the accelerating electrode is $U_{ex} = -20$ kV. The amplitude and time parameters of the discharge current (I_d) and the ion current extracted from PIS (I_{ex}) were measured depending on the gas pressure. The pulsed operation modes, the current delay (t_{delay}) and rise time (t_{front}) of extracted current were measured (see figure 5). The current delay time is define as the time between rising edge of anode voltage and rising edge of current pulse (10% of the plateau). The t_{front} is associated with the rise of the current pulse (from 10% to 90% of the plateau). The amplitude-time characteristics of the discharge and extracted currents were investigated as a function of magnetic field induction (and configuration) in the pulse power supply mode of anode voltage. Experiment goal aims were maximum ion-extraction coefficient (the ratio of the extracted current to the discharge current I_{ex}/I_d) at the lowest pressure and rectangular form of extracted ion current (minimum of t_{front} and t_{delay}).

The I_{ex} and I_d amplitudes are plotted as functions of pressure in the discharge cell for different solenoid positions and coil current upon the measured current pulse waveforms: (a) $I_{coil} = 8$ A (see figures 7(a) and (b) $I_{coil} = 10$ A (see figure 7(b)). These coil currents demonstrate the fundamental influence of the magnetic field induction (‘low’ $B_z < 90$ mT or ‘high’ $B_z > 90$ mT) and its distribution (homogenous and inhomogeneous) on the general dependence of the current pulse on the working gas pressure.

As it can be seen from figures 6(a) and 7(a), for low ($B_z < 90$ mT) and homogenous ($l = 0$ –5 mm) magnetic fields the discharge parameters and extraction current characteristic

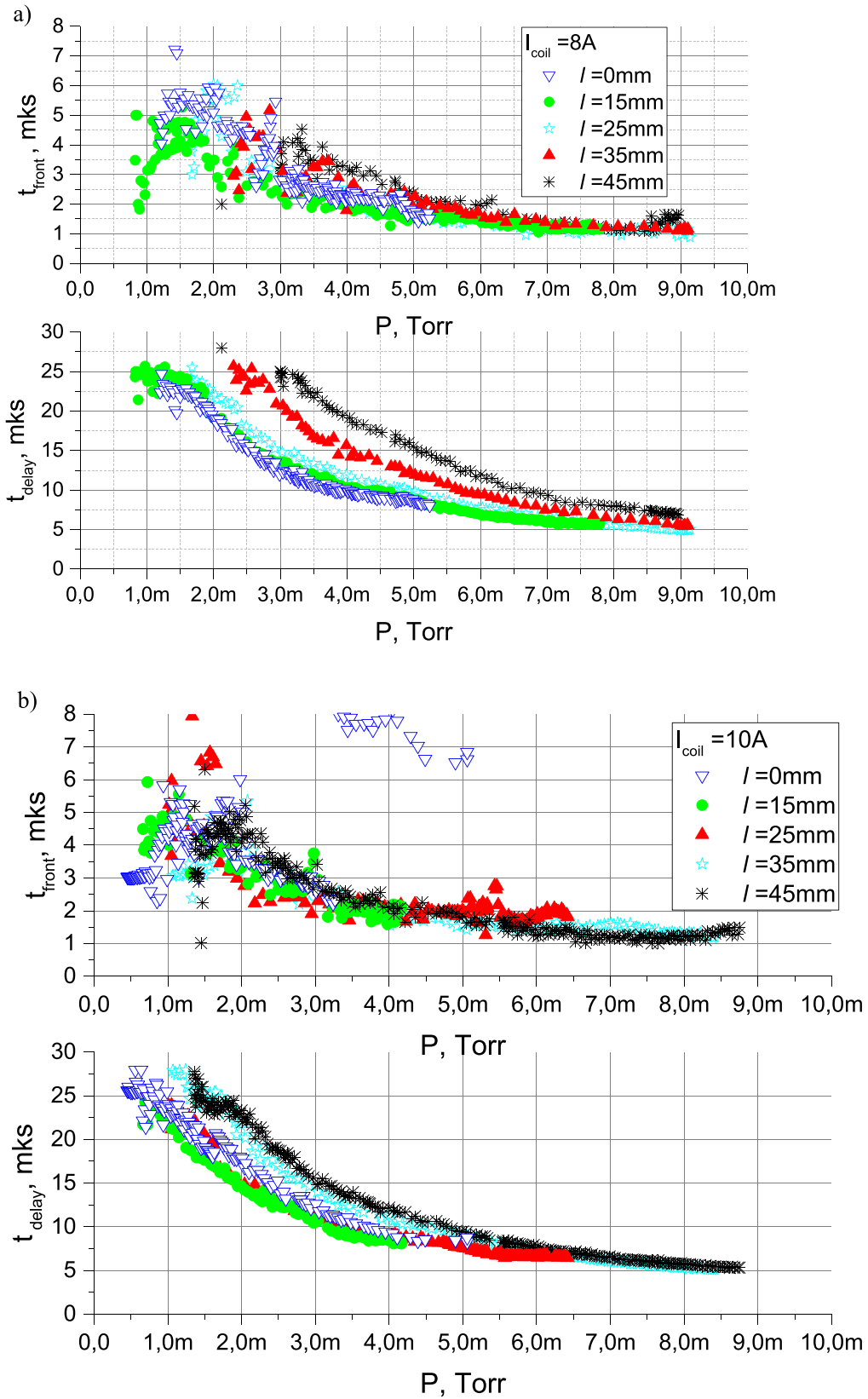


Figure 9. Delay t_d , and rise t_{front} time, as a function of pressure for different solenoid positions and coil current: (a) $I_{coil} = 8 A$ and (b) $I_{coil} = 10 A$.

Table 1. Discharge mode change depending on the magnetic field induction and configuration.

Magnetic field induction	Magnetic field homogeneity		
	Homogenous	Lightly inhomogeneous	Strongly inhomogeneous
	$(l = 0-5 \text{ mm})$	$(l = 15-25 \text{ mm})$	$(l = 35-45 \text{ mm})$
Low (65–90 mT)	—High discharge currents; —No significant increase in the extracted current towards high pressure $I_d \geq 1 \text{ mA}$ $I_{ex} \sim 0.2-0.5 \text{ mA}$ $t_{delay} \rightarrow 7 \mu\text{s}$ $t_{front} \rightarrow 1.5 \mu\text{s}$	—Low discharge currents; —Quasi-rectangular form of extracted pulse $I_d \sim 0.5 \text{ mA}$ $I_{ex} \sim 0.2-0.5 \text{ mA}$ $t_{delay} \rightarrow 5 \mu\text{s}$ $t_{front} \rightarrow 1 \mu\text{s}$	—Low discharge currents —Dependence $I_d(p)$ and $I_{ex}(p)$ drift towards high pressure $P \rightarrow 3 \text{ mTorr}$, $I_d \sim 1 \text{ mA}$ $I_{ex} \sim 0.2-0.5 \text{ mA}$ $t_{delay} \rightarrow 5 \mu\text{s}$ $t_{front} \rightarrow 1 \mu\text{s}$
High (90–120 mT)	—Transition to HMF mode is possible, —Time characteristic deterioration —Triangular shape of discharge pulse $I_d \sim 0.8-10 \text{ mA}$ $I_{ex} \sim 0.2-0.5 \text{ mA}$ $t_{delay} \rightarrow 7 \mu\text{s}$ $t_{front} \rightarrow 1.5 \mu\text{s}$	—Shorter delays in whole pressure range —Triangular bursts in the discharge —Triangular shape of discharge pulse $I_d \sim 0.4-4 \text{ mA}$ $I_{ex} \sim 0.2-0.5 \text{ mA}$ $t_{delay} \rightarrow 5 \mu\text{s}$ $t_{front} \rightarrow 1.5 \mu\text{s}$	—Drift of burning region $P < 1 \text{ mTorr}$, —Earlier transition to TM burning mode $P \sim 2 \text{ mTorr}$ —Triangular shape of discharge pulse $I_d < 0.4-4 \text{ mA}$ $I_{ex} \sim 0.2-0.5 \text{ mA}$ $t_{delay} \rightarrow 7 \mu\text{s}$ $t_{front} \rightarrow 1.5 \mu\text{s}$

are essentially dependent on the magnetic field. At the voltage pulse duration $t_{vp} = 30 \mu\text{s}$ discharge are not ignited in magnetic fields less than 65 mT. Then, as the B_z increases the current time delay decreases and discharge (and extraction) current increases at the same pressure. There is a trapezoidal shape of the discharge current pulses (and quasi-rectangular shape of extraction current pulses) for $B_z \sim 70-80 \text{ mT}$ and starting from 2 to 3 mTorr. The conditions of discharge ignition with explicit flat peak of the extracted current pulse are implemented in the pressure range $P = 5-6 \text{ mTorr}$, while the current delay time does not exceed $10 \mu\text{s}$. There are typical triangular bursts in the discharge with frequency of about hundreds kHz to several MHz for magnetic field less than 70 mT in all operating pressure range. The current delay time t_{delay} is 15–20 μs . A similar form of current pulses is obtained for homogeneous fields above 90 mT. While increasing magnetic field induction ($B_z > 90 \text{ mT}$), the discharge mode in the PIS changes and is accompanied with high discharge current pulse amplitude while other parameters remain unchanged. In this mode, the discharge current goes monotonically up for pulse time so that the maximum current at the pulse end reached $I_d = 4-5 \text{ mA}$. At the same time, the extracted current pulse had the typical triangular bursts of up to 0.8 mA height. A further pressure rise ($>5-7 \text{ mTorr}$ —pressure range depending on the magnetic field) causes an exponential increase in the discharge current (above 1 mA).

By analogy with the initial [18, 19], it can be assumed that such instability (oscillations) of the discharge current is caused by fluctuations between adjacent discharge mode. The discharge switches from LMF mode to TM-mode with possible the discharge current fall. Estimates of the ion Larmor (cyclotron) radius show that the magnetic field in the range $\sim 100 \text{ mT}$ does not affect the movement of the ions, if it is

consider independently of the electron component. The characteristic ion Larmor radius (i.e. protons with max $W = 2 \text{ kV} = e \cdot U_a$ (anode voltage), $B = 100 \text{ mT}$, yielding Larmor radius $\sim 6 \text{ cm}$) is significantly larger than the discharge cell size ($\sim 1.5 \text{ cm}$). Therefore, the ions move almost freely (the collisionality is relatively weak since the ion mean free path length ($\sim 0.7 \text{ cm}$) is of the order of the discharge cell size ($\sim 1.5 \text{ cm}$)) to the cathode along the electric field lines, without the direct influence of the magnetic field. (So there is no direct way influence of the magnetic field on ion movement.) In contrast the magnetic field significantly affects the electron component resulting in a space-charge formation which massively changes the pattern of the electric field lines. In turn the changes in the electric field affect the movement of the ions. A further pressure rise leads to transition to the high-pressure mode—HP with an exponential increase of the discharge current. In figure 7 pressure point of discharge mode transition (TM \rightarrow HP) depends on magnetic field value and configuration.

When induction of the uniform magnetic field exceeds $\sim 100 \text{ mT}$ (see figures 7(b) and 8), the discharge changes to HMF mode. The features of this mode are a potential fall on the discharge volume axis to the cathode (i.e. zero) value and maximum discharge current during transition from LMF mode to HMF mode. There is a delay between discharge current pulse and extracted current. This fact can be explained in the following way: the potential fall on the axis causes generation of zero axial field, $E_z = 0$, which can cover the whole cell. The ionization region is shifted for some distance in the radial direction from the axis. So, the ions generated start radial oscillations and slowly drift along z -axis with thermal velocities. The ions graze on the cathodes and in some cases (see [26, 27]) miss the cathode center at all. This

fact can explain the low ion extracted current against the discharge current. There was also a time delay (5–10 μs) between the discharge current pulse start and extraction current pulse start.

The results obtained show that the solenoid shift towards cathode (i.e. generation of inhomogeneous magnetic field linearly decreasing to the anticathode) causes a current drift to the higher pressures. Transition from the homogenous magnetic field to the inhomogeneous one changes the discharge burning mode: high magnetic field (HMF) mode is replaced with the low magnetic field (LMF) mode. The homogenous magnetic field allows discharge currents to reach high values, while the extracted current increases slightly. An extension of field inhomogeneity shifts the discharge ignition region to the pressure range of 1–2 mTorr. At the same time the pressure goes up so that the discharge changes to burning mode characterized by a drastic discharge current rise ('transition' mode (TM)).

Figure 9 shows the time dependences of t_{delay} and t_{front} on the pressure when the magnetic field varies in the cell. As you can see, the shorter delay times are specific for insignificant inhomogeneity of the magnetic field (shift $l = 15$ mm) for the whole pressure range. The rise time within the error slightly depends on the field configuration, in contrast to the current pulse delay.

Thus, in contrast to [28, 29], the results obtained here suggest that the induction and configuration of the magnetic field have a significant effect on the discharge ignition time. Table 1 presents the main conclusions on the discharge mode change depending on the magnetic field induction and configuration.

5. Conclusion

The magnetic field distributions in the PIS were calculated using the COMSOL software and measured with induction coils. The obtained simulation data shows the possible configurations of the magnetic field distribution depending on the solenoid position along the axis of PIS. Discharge and extracted currents were experimentally studied as a function of the magnetic field (both homogenous and inhomogeneous) induction, the working gas pressure, and the anode voltage in the pulsed power supply modes of PIS. The experiments showed a significant effect of the magnetic field induction and structure on the pressure range of the gas with stable discharge ignition, as well as the amplitude and time characteristics of the discharge and extracted currents. Homogeneous magnetic field ($B_z \approx 90$ mT) increased the amplitude values of discharge current, but there was no significant decrease t_{delay} . Homogeneous magnetic field ($B_z > 100$ mT) led to a change combustion discharge mode. Discharge current pulse reached values more than 8 mA, at the same time extraction current was about 0.3 mA. Inhomogeneous magnetic field with a linearly decreasing magnetic induction value (from cathode to anticathode) improved the current pulse time characteristics, decreased discharge current and increased extraction coefficient. In these magnetic field the current pulse

of the extracted ions had a quasi-rectangular form and with pressure increases (in range 2–6 mTorr) the extracted current amplitude linearly increases from 200 to 400 μA , the current pulse delay decreases from 10 to 5 μs , and the rise time decreases from 2 to 1 μs .

Acknowledgments

The authors would like to thank Dr A A Pshenov from 'NRC Kurchatov Institute' for the help and useful discussions.

ORCID iDs

N V Mamedov  <https://orcid.org/0000-0002-5052-7594>

V I Zverev  <https://orcid.org/0000-0002-6977-2143>

S P Maslennikov  <https://orcid.org/0000-0001-5888-824X>

References

- [1] Penning F M and Moubis J H A 1937 *Physica* **4** 71–6
- [2] Valkovic V 2016 *14 MeV Neutrons. Physics and Applications* (Boca Raton, FL: CRC Press Taylor and Francis) pp 500
- [3] Schuurman W 1967 *Physica* **36** 136–60
- [4] Hooper E B 1969 A Review of Reflex and Penning Discharges *Advances in Electronics and Electron Physics* vol 27 (New York: Academic) pp 295–343
- [5] Sy A, Ji Q, Persaud A, Waldmann O and Schenkel T 2012 *Rev. Sci. Instrum.* **83** 02B309
- [6] Kolodko D V et al 2017 *Phys. At. Nucl.* **80** 1687–91
- [7] Mahjour-Shafiei M, Noori H and Ranjbar A H 2011 *Rev. Sci. Instrum.* **82** 113502
- [8] Fathi A, Fegghi S A H, Sadati S M and Ebrahimibasabi E 2017 *Nucl. Instrum. Methods Phys. Res. A* **850** 1–6
- [9] Kolodko D V et al 2015 *Phys. Proc.* **71** 150–4
- [10] Dolgov A N et al 2016 *J. Phys.: Conf. Ser.* **666** 012023
- [11] Li G, Zhang Z, Chi Q and Liu L 2012 *Nucl. Instrum. Methods Phys. Res. B* **290** 64–8
- [12] Rovey J L 2008 *Plasma Sources Sci. Technol.* **17** 035009
- [13] Liu W, Li M, Gao K and Gu D 2014 *Nucl. Instrum. Methods Phys. Res. A* **768** 120–3
- [14] Yan F, Jin D, Chen L, Wan X and Xiang W 2018 *IEEE Trans. Plasma Sci.* **46** 2546–9
- [15] Yan F, Jin D, Chen L and Xiao K 2018 *Nucl. Inst. Methods Phys. Res. A* **906** 110–3
- [16] Bernander H, Codechot X L M and Lejeune C A 1992 Device for perfecting an ion source in a neutron tube *US Patent* 5 104 610
- [17] Li M, Xiang W, Xiao K X and Chen L 2012 *Rev. Sci. Instrum.* **83** 02B722
- [18] Mamedov N V et al 2016 *J. Phys.: Conf. Ser.* **755** 011001
- [19] Mamedov N V et al 2018 *Tech. Phys.* **63** 1129–36
- [20] Mamedov N V et al 2018 *Instrum. Exp. Tech.* **61** 530–7
- [21] Rachkov R S, Presnyakov A Y and Yurkov D I 2019 *At. Energy* **126** 383–7
- [22] Mamedov N V et al 2019 *Tech. Phys.* **64** 1290–7
- [23] Liberman A D and Chen F K 1995 Neutron-burst timing with sealed tube generators *Proc. SPIE* **2339** 188–95
- [24] Radtke R J et al 2012 A new capture and inelastic spectroscopy tool takes geochemical logging to next level *Proc. SPWLA 53rd Annual Logging Symp.*

- [25] Petrovich E P, Sergeevich V V and Halimovich Y R 2008 Gas-filled neutron pipe *Federal State Unitary Enterprise Russian patent 2366030* (https://yandex.ru/patents/doc/RU2366030C1_20090827)
- [26] Knauer W 1966 *J. Appl. Phys.* **37** 602
- [27] Knauer W 1962 *J. Appl. Phys.* **33** 2093–9
- [28] Burns E and Bischoff G 1997 *AIP Conf. Proc.* **392** 1207–10
- [29] Chen F K 1984 *J. Appl. Phys.* **56** 3191–7